Kinetic Analysis of Isothermal Crystallization of Potassium Aluminosilicate Ceramics (Leucite and Kalsilite) from Amorphous Potassium Aluminosilicate Precursors

ARTICLE *in* CRYSTAL GROWTH & DESIGN · FEBRUARY 2010

Impact Factor: 4.89 · DOI: 10.1021/cg901194k

8 AUTHORS, INCLUDING:

Iva Buljan
Ruđer Bošković Institute
7 PUBLICATIONS **26** CITATIONS
SEE PROFILE

Natasa Novak Tusar
National Institute of Chemistry
75 PUBLICATIONS **552** CITATIONS
SEE PROFILE

Alenka Ristic
National Institute of Chemistry
58 PUBLICATIONS **428** CITATIONS
SEE PROFILE

Tea Mišić Radić
Ruđer Bošković Institute
20 PUBLICATIONS **162** CITATIONS
SEE PROFILE

DOI: 10.1021/cg901194k

CRYSTAL GROWTH & DESIGN Article

2010, Vol. 10 838–844

Kinetic Analysis of Isothermal Crystallization of Potassium Aluminosilicate Ceramics (Leucite and Kalsilite) from Amorphous Potassium Aluminosilicate Precursors

Iva Buljan,[†] Cleo Kosanović,*[,†] Boris Subotić,[†] Nataša Novak Tušar,[‡] Alenka Ristić,[‡] Roman Gabrovšek,[‡] Venčeslav Kaučič,[‡] and Tea Mišić Radić[†]

[†]*Ruđer Bošković Institute, Bijenička 54, 10000 Zagreb, Croatia and* [‡]*National Institute of Chemistry, Hajdrihova 19, 1000 Ljubljana, Slovenia*

Received September 29, 2009; Revised Manuscript Received December 18, 2009

ABSTRACT: Kinetics of the isothermal crystallization of tetragonal modification of leucite and hexagonal modification of kalsilite from differently prepared precipitated amorphous aluminosilicate precursors were investigated at three different temperatures. Kinetic analyses of the transformation processes have shown that the crystallization of leucite occurs the same way as the crystallization of kalsilite and follows a pseudo-zero-rate kinetic equation. The apparent activation energies calculated by the Arrhenius equation were 373 kJ/mol for the crystallization of kalsilite and 403 kJ/mol for the crystallization of leucite, which is explained by the different microstructures of the prepared precursors.

1. Introduction

Starting from the pioneering work of Mimura and Kanno,[1] the possibility of the preparation aluminosilicate-based ceramic materials by high-temperature, solid-state transformations of zeolites and their cation-exchanged derivatives was the objective of intensive investigations during the last two decades.[2−11]

Detailed phase analyses during the transformations have shown that the transformation process takes place in two steps:[1,2,7,9−14] (i) formation of X-ray amorphous aluminosilicate having the same chemical composition as the starting crystalline precursor (zeolite) and (ii) formation of secondary crystalline phase (aluminosilicate-based ceramic) by its crystallization from the amorphous aluminosilicate obtained in the first step of the process.

Generally, the temperature of transformation in each of the steps, pathways of the processes, and structural and chemical properties of the aluminosilicate-based ceramics formed in the second step of the overall transformation process strongly depend on the type of zeolite used as precursor and its chemical composition, for example, SiO_2/Al_2O_3 ratio[1,15,16] and especially, the type of compensating cation.[1,2,4,7,11,12]

Kinetic analyses of particular transformation steps (amorphization of zeolite precursor, crystallization of the secondary crystalline phase) and the solution of the population balance of the entire transformation process have shown that[11,17] (i) amorphization of zeolite takes place by a random, diffusion-limited agglomeration of the short-range-ordered aluminosilicate subunits formed by thermally induced breaking of Si−O−Si and Si−O−Al bonds between different building units of the zeolite framework, and (ii) crystallization of secondary crystalline phase (ceramic) occurs by homogeneous nucleation of ceramic material inside the matrix of amorphous aluminosilicate and diffusion-controlled growth of the nuclei. The growth is one-dimensional in the case of transformation of zeolite 4A (sodium form of zeolite A) into low-carnegieite, which causes formation of needle-shaped crystals of low-carnegieite.[10,11,17]

Analysis of the particulate properties (particle size, particle shape) of the solid phases during high-temperature, solid-state transformations of the ammonium form of zeolites A and X into mullite[9,14] and the potassium form of zeolite A into kalsilite and kaliophilite[12,13] have shown that despite the intensive structural changes (zeolite → amorphous → ceramic) the obtained intermediate (amorphous aluminosilicate) and the final product (aluminosilicate-based ceramic) have the same size and shape as the starting zeolite powder (pseudomorphism).[18] This indicates that all the above-mentioned events relevant for solid-state transformation (amorphization of zeolite, nucleation and crystal growth of secondary crystalline phase − ceramic) occur inside each single particle[11,17] which can be seen as a "closed" microreactor with a stable shell.[13,14] Since microcrystals of the formed secondary crystalline phase (ceramic) are distributed inside single particles (microreactors) having "smooth" outer surfaces (shell),[9,12−14] the size and shape of the microcrystals of the secondary crystalline phase cannot be determined by a direct (microscopic) observation. On the other hand, the fact that the process of transformation does not occur in a direct way, that is, by reorganization (rotation and/or translation) of primary and secondary building units of zeolite framework into secondary crystalline phases (aluminosilicate-based ceramics), but that nucleation and crystal growth of the secondary crystalline phase takes place by reaction of primary building units (SiO_4 and AlO_4 tetrahedra) of the amorphous phase,[7,9,11−17] indicates that not only zeolites but also precipitated amorphous aluminosilicates (gels) can be transformed into aluminosilicate-based ceramics. This thesis was recently confirmed by the analysis of the changes of the phase and particulate properties during high-temperature, solid-state transformation of precipitated X-ray amorphous sodium-aluminosilicate (Na-gel) into low-carnegieite.[10] The mechanism of crystallization is the same as the mechanism of crystallization of low-carnegieite from zeolite 4A (sodium

*To whom correspondence should be addressed. Tel.: +385-1-4680-236. E-mail: cleo@irb.hr.

 Published on Web 01/12/2010

form of zeolite A), homogeneous nucleation of low-carnegiete inside the matrix of Na-gel and diffusion-controlled, one-dimensional growth of the nuclei.[10,11,17] In contrast to the impracticability of the direct observation of the microcrystals of the secondary crystalline phase formed in "closed" microreactors, the microcrystals of the secondary crystalline phase formed on the surface of gel may be directly observed by appropriate microscopic techniques. Scanning-electron micrographs of the crystalline end product obtained by heating of the Na-gel showed that rhombohedric modification of low-carnegieite crystallizes in the form of needles,[10] as previously predicted on the basis of the kinetic analysis of transformation of zeolite A into low-carnegieite.[11,17]

Since zeolite 3A (potassium form of zeolite A) can be transformed into a mixture of kalsilite and kaliophilite by a high-temperature, solid-state pseudomorphic process in the sequence: zeolite 3A → X-ray amorphous potassium aluminosilicate → kalsilite + kaliophilite,[7,12,13] it is reasonably to assume that also the precipitated, X-ray amorphous potassium aluminosilicate can be directly transformed into kalsilite, kaliophilite, and/or their mixtures. Hence, the objectives of this study are

(1) To prove (or disapprove) the thesis that kalsilite, kaliophilite, and/or other K-aluminosilicate-based ceramics (e.g., leucite) can be obtained by a thermal treatment of precipitated, X-ray amorphous potassium aluminosilicate
(2) To observe (by appropriate microscopic techniques) the size and shape of the resulting crystalline phase(s)
(3) To determine the mechanism of assumed crystallization of the mentioned K-aluminosilicate-based ceramics from the precipitated, X-ray amorphous potassium aluminosilicate
(4) To compare the mechanism of transformation of the precipitated, X-ray amorphous potassium aluminosilicate into crystalline ones with the previously defined mechanism of crystallization of low-carnegieite from Na-gel

2. Experimental Section

2.1. Preparation of K-Aluminosilicate Hydrogels and Amorphous K-Aluminosilicate Precursors (Gels). K-aluminosilicate hydrogels and the corresponding amorphous K-aluminosilicate precursors [K-gel(A), K-gel(B)] were prepared by two different procedures, as follows:

Procedure (A): by the ion-exchange of sodium ions from Na-aluminosilicate gel with NH_4^+ and then with potassium cation resulting in K-gel(A) and

Procedure (B): by direct precipitation from K-aluminate and K-silicate solutions resulting in K-gel(B). The synthesis procedure is described in detail in ref 16.

2.2. Thermal Treatment of Gels. In order to transform the dried gels, prepared by the described procedures (A and B ref 16) into ceramics, the gel samples were put into small quartz tubes (l = 2.5 cm, ϕ = 2 cm) and then isothermally heated at three different temperatures T (= 1423 K, 1453 K 1483 K) in a chamber furnace with controlled temperature (ELPH-2, Elektrosanitarij), for appropriate times t in the interval from $t = 0$ to $t = t$(end) (the time after further structural changes are not detected). At various times, t, after the beginning of heating at elevated temperature, the samples were taken from the furnace and cooled down in a desiccator over dry silica gel in order to stop the transformation process and prepare the samples for analysis. The zero time of the transformation process ($t = 0$) was taken as the moment when the sample is put in the furnace preheated at the transformation temperature T.

2.3. Characterization/Analyzes of the Samples. The gels K-gel(A) prepared by Procedure A, the gel K-gel(B) prepared by Procedure B, and the crystalline products obtained by their thermal treatment (see section 2.2) were characterized/analyzed as follows:

Chemical composition of the amorphous (gels) and crystalline samples (ceramics) were determined by energy dispersive X-ray spectroscopy (EDS) technique using the LINK ISIS 300 system attached to the scanning-electron microscope JEOL JSM-5800.

The water content was determined by thermogravimetry (TG) performed on a SDT 2960 thermal analysis system (TA Instruments Inc.). The measurements were carried out in nitrogen atmosphere with a heating rate of 10 °C/min.

X-ray powder diffraction patterns of all solid samples (gels and ceramics) were taken using a PANalytical X'Pert PRO high-resolution diffractometer with Alpha 1 configuration using $CuK_{\alpha 1}$ radiation (0.15406 nm) in the 2θ range from 5 to 55 °2θ using a step of 0.017 °2θ per 100 s.

The weight fractions, $f_{gel(A)}$ of K-gel(A), $f_{gel(B)}$ of K-gel(B), f_{ck} of kalsilite, and f_{cl} of leucite were calculated by a combination of Hermans-Weidinger[19] and mixing method.[20]

The specific surface area of the solid samples was determined by multiple point nitrogen adsorption (BET method) in the relative pressure range from 0.05 to 0.25, using a TriStar 3000 Micromeritics instrument. Prior to the measurement, the samples were outgassed at 100 °C for 1 h to desorb the loosely held moisture from the outer surface of the samples.

Scanning-electron micrographs of the samples were taken by a JEOL JSM 7000F scanning-electron microscope.

Atomic force microscope (AFM) imaging was performed using a multimode scanning probe microscope with a Nanoscope IIIa controller (Veeco Instruments, Santa Barbara, CA) with a vertical engagement (JV) 125 μm scanner. The samples were prepared as follows: The powdered samples were suspended in ultrapure water (1 g/L) and stirred for 1 h. Final suspension contained 10 mg of powder/L. Five microliters of the final suspension was pipetted directly onto freshly cleaved mica. Following deposition, the mica sheets were placed in enclosed Petri dishes for several hours at a relative humidity of 50% in order to evaporate the excess of water. Images were collected using tapping mode AFM because it is particularly well adapted to soft samples due to a nearly complete reduction of lateral forces. "Light tapping" was applied using silicon tips (TESP, Veeco).

3. Results and Discussion

Although the aluminosilicate composition of starting hydrogels, defined by the batch molar ratios $[Me_2O/Al_2O_3]_b$ = 3.55, $[SiO_2/Al_2O_3]_b$ = 2.26, and $[H_2O/Al_2O_3]_b$ = 153.47 (Me = Na, K), was the same for sodium- and potassium-aluminosilicate hydrogel (see Experimental in ref 16), chemical analysis of the separated solid phases (gels) showed that aluminosilicate composition of K-gel(B) [$1.01K_2O\cdot Al_2O_3\cdot 3.31SiO_2\cdot 12.53H_2O$] considerably differs from the chemical composition of Na-gel(A) [$1.03Na_2O\cdot Al_2O_3\cdot 2.58SiO_2\cdot 4.07H_2O$]. The molar ratio Me_2O/Al_2O_3 is very close to 1 in both the gels; that is, Na_2O/Al_2O_3 = 1.03 for Na-gel(A) and K_2O/Al_2O_3 = 1.01 for K-gel(B). This indicates that Al in the skeleton of amorphous aluminosilicate gel is coordinated 4-fold within the common (Si,Al,O)-framework,[21−23] whereas the Me^+ ions compensate excess negative charges of aluminum−oxygen tetrahedral.[21] On the other hand, the higher molar ratio SiO_2/Al_2O_3 (= 3.31) in K-gel(B) relative to the molar ratio SiO_2/Al_2O_3 (= 2.58) in Na-gel(A) (= 2.58) is obviously affected by the nature of cation Me, as explained in a previous study.[16]

The molar ratios Me_2O/Al_2O_3 and SiO_2/Al_2O_3 of the Na-gel(A) does not considerably change during the exchange of the host Na^+ ions with NH_4^+ ions from solution as well as during the exchange of NH_4^+ ions from the solid NH_4-gel(A) with K^+ ions from solution (see Experimental ref 16), so that

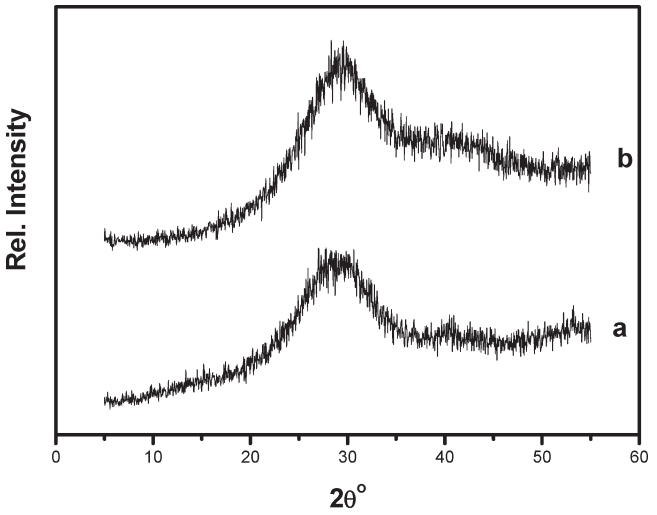

Figure 1. X-ray diffraction (XRD) patterns of the amorphous aluminosilicate precursors prepared by Procedure A, K-gel(A) (a) and Procedure B, K-gel (B) (b).

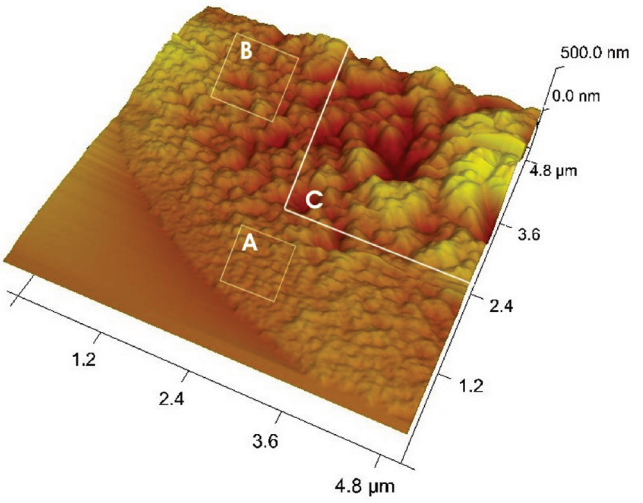

Figure 2. AFM image, 3D presentation of height data of K-gel(A).

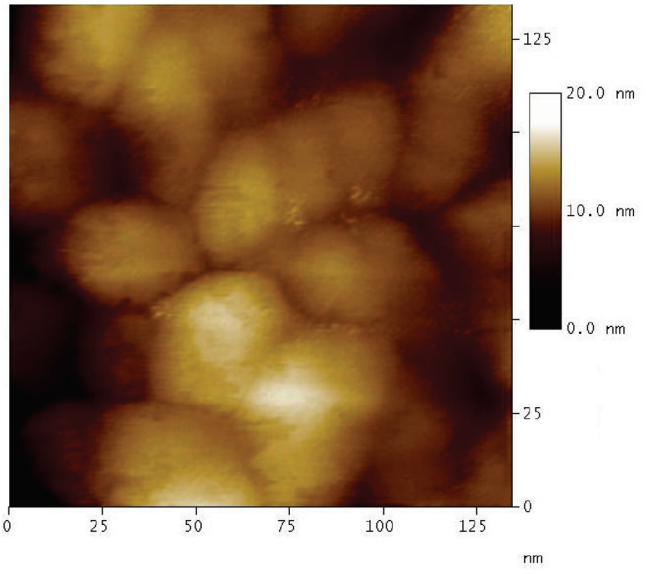

Figure 3. Typical AFM image of the K-gel(B) elemental particle in clusters.

the aluminosilicate composition of K-gel(A) ($0.96K_2O \cdot 0.08Na_2O \cdot Al_2O_3 \cdot 2.65SiO_2 \cdot 3.28H_2O$) is closer to the aluminosilicate composition of Na-gel(A) than to the aluminosilicate composition of K-gel(B). This can be easily explained by the fact the exchange processes (Na^+ by NH_4^+ and NH_4^+ by K^+; see Experimental in ref 16) represent simple replacements of compensating cations without their chemical interactions with aluminosilicate framework.

Results of X-ray diffraction analysis of the potassium aluminosilicate gel precursors K-gel(A) and K-gel(B) show that regardless of the differences in chemical composition (see above) as well as surface and microstructural properties (see below), the X-ray diffraction patterns of both the gels are almost the same (see Figure 1) and characteristic for precipitated amorphous aluminosilicates.[24−27]

High BET specific surface area of the X-ray amorphous precursors K-gel(A) (53 m^2/g) and K-gel(B) (183 m^2/g) are the consequence of the great internal surfaces of these amorphous phases caused by their (micro/meso)-porous nature.[28−30] However, due to a higher content of water,[16] the gel K-gel(B) is more porous than the gel K-gel(A), and thus the BET specific surface area of the gel K-gel(B) is about 3.5 times higher than the BET specific surface area of the gel K-gel(A).

Previous atomic force microscopy (AFM) studies of amorphous aluminosilicate gels[30,31] have shown that this method, which (i) produces the image of material with vertical resolution as small as 0.1 nm and with lateral resolution superior to 1 nm, (ii) provides a true three-dimensional surface profile and (iii) does not require some special treatments (such as metal coatings) that would irreversibly change and/or damage the sample, is a powerful tool for investigation of microstructural properties of amorphous aluminosilicate gels. For this reason, microstructural properties of the X-ray amorphous aluminosilicate precursors K-gel(A) and K-gel(B) were additionally examined by the AFM method. AFM image in Figure 2 shows that X-ray amorphous aluminosilicate precursor K-gel(A) contains three different types of nanosized entities: (A) disk-shaped particles, (B) "transition", probably partially crystalline, features (particles of "quasi-crystalline" phase,[29] and (C) "pyramidal-shape" features which look like fully crystalline material. The same three types of the nanosized entities were previously found in X-ray amorphous sodium aluminosilicate gel[30] having the same chemical composition as Na-gel(A). This indicates that double exchange process [Na-gel(A) → NH_4-gel(A) → K-gel(A)] does not affect either aluminosilicate composition of the gel (see above) or its microstructural properties. In contrast to "complex" microstructural features of Na-gel(a) and K-gel(A), respectively, the AFM image in Figure 3 shows that K-gel(B) represents aggregates composed of the nanosized entities of type (A) only. Detailed section analysis of the disk-shaped particles [type (A)][30] has shown that the nanosized entities of type (A) have a diameter in the range from 20 to 50 nm and height from 3.5 to 8 nm and without some "structural" particularities. Thus, it was concluded that the nanosized entities of type (A) represent the primary amorphous gel particles.[30] The presence of ordered crystalline phase in the gel matrix of the precursor Na-gel(A) → K-gel(A) (Figure 2) is connected with the ability of the "structure forming" Na^+ ions to form structural subunits[33−36] or even more complex structures, resembling those in crystalline products, inside the gel matrix during its formation.[16,36,37] By the same principle, the absence of structurally ordered

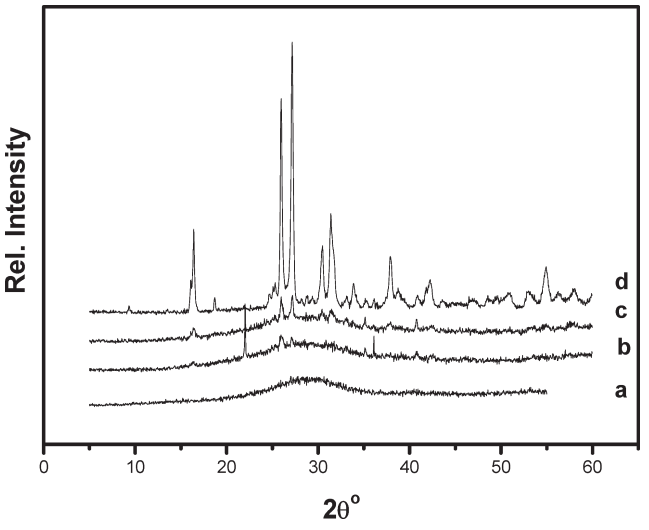

Figure 4. X-ray diffraction patterns of the solid phases obtained by thermal treatment of K-gel(A) (a) at 1483 K for 0.5 h (b), 2 h (c), and 5 h (d).

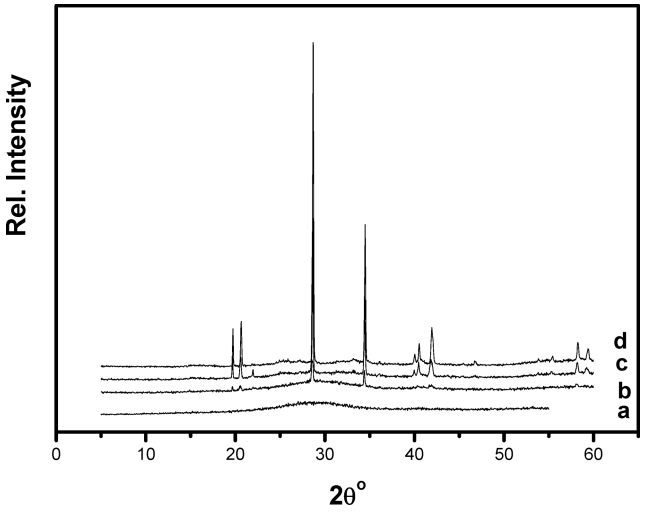

Figure 5. X-ray diffraction patterns of the solid phases obtained by thermal treatment of K-gel(B) (a) at 1483 K for 0.5 h (b), 1 h (c), and 2 h (d).

entities in the matrix of K-gel(B) can be readily explained by the absence of the "structure forming" Na^+ ions, and the presence of "structure breaking" K^+ ions[16,32−37] in the batch, during formation (precipitation) of the K-gel(B).

Now, taking into consideration differences in chemical composition, surface, and microstructural properties of the X-ray amorphous aluminosilicate precursors K-gel(A) and K-gel(B), it is reasonably to assume that thermal treatment of the precursors would result in different results. X-ray diffraction patterns of the solids obtained during heating of K-gel(A) (Figure 4) and K-gel(B) (Figure 5) confirm such an assumption; thermal treatment of K-gel(A) results in a gradual transformation of X-ray amorphous phase (see X-ray diffraction patterns a in Figures 1 and 4) into leucite (see X-ray diffraction patterns b−d in Figure 4), and thermal treatment of K-gel(B) results in a gradual transformation of X-ray amorphous phase (see X-ray diffraction pattern b in Figure 1 and X-ray diffraction pattern a in Figure 5) into kalsilite (see X-ray diffraction patterns b−d in Figure 5). Phase and chemical analysis, respectively, of the final products of transformations have shown that the final product of transformation of K-gel(A) contains about 80 wt% of leucite, and the rest is potassium and/or sodium aluminate and that the final product of transformation K-gel(B) contains about 85 wt% kalsilite, and the rest is silica and traces of potassium silicate. The incomplete transformation of amorphous precursor into a corresponding crystalline phase, previously observed during transformation of Na-gel into low-carnegieite,[10] is caused by the fact that the Si/Al ratio of precursor is different than the Si/Al ratio of product (ceramic). For example, the molar ratio Si/Al of K-gel(A) is 1.29 and the molar ratio Si/Al of the resulting leucite ($KAlSi_2O_6$) is 2, and hence the content of silicon in K-gel(A) determines the amount of the formed leucite. On the other hand, the molar ratio Si/Al of K-gel(B) is 1.65 and the molar ratio Si/Al of the resulting kalsilite ($KAlSiO_4$) is 1, and hence the content of aluminum in K-gel(A) determines the amount of the formed kalsilite. Since higher-silica leucite ($KAlSi_2O_6$) was crystallized from lower-silica K-gel(A) and lower-silica kalsilite ($KAlSiO_4$) was crystallized from higher silica K-gel(B), it is evident that the type of product is determined rather by the microstructural properties of precursor than by its chemical composition. However, the relationship between the microstructural properties of the precursor and the type of product (ceramic) obtained by its thermal treatment is not clear at present.

The scanning-electron micrographs of the final products obtained by thermal treatment of K-gel(A) and K-gel(B) at 1483 K presented in Figure 6 show that the product of transformation is composed of aggregates of very small particles (about 10 nm). On the other hand, the analysis of X-ray diffraction patterns using the Scherrer equation shows that the crystal size of leucite is 32 nm and the size of kalsilite is 117 nm. This means that the very small (about 10 nm) particles that "cover" the leucite and/or kalsilite crystals (see Figure 6) probably represent byproducts (a mixture of sodium and potassium aluminate in the case of leucite and potassium silicates and silicon dioxide in the case of kalsilite); these byproducts arise from the differences in the chemical compositions between starting gels and final products, that is, K-gel(A): $[(0.96K_2O\cdot 0.08Na_2O)\cdot Al_2O_3\cdot 2.65SiO_2\cdot 3.28H_2O] \rightarrow 2KAlSi_2O_6 + 0.24NaAlO_3 + 0.89KAlO_3$; K-gel(B): $[1.01K_2O\cdot Al_2O_3\cdot 3.31SiO_2\cdot 12.53H_2O] \rightarrow 2\ KAlSiO_4 + 0.01\text{-}K_2SiO_3 + 1.29SiO_2$.

Kinetics of transformation of K-gel(A) into leucite is shown in Figure 7 and the kinetics of transformation of K-gel(B) into kalsilite is shown in Figure 8. As expected,[10,11,17] in both the cases, the rate of transformation increases with increasing transformation temperature T, but for a given temperature T, the rate of transformation of K-gel(B) into kalsilite is higher than the rate of transformation of K-gel(B) into leucite. Generally, the rate of transformation, df_c/dt can be expressed as[10,11,17,39−41]

$$df_c = G\sigma[L(\tau, t)]^n(dN/d\tau)d\tau \quad (1)$$

where f_c is the mass fraction of the crystalline phase (ceramic) formed during isothermal transformation process, $L(\tau,t)$ is the crystal size which depends on the time τ in which the nucleus is formed and starts to grow and the time of crystallization t, $dN/d\tau$ is rate of nucleation, G is the geometrical factor of particle (crystal) shape, σ is the density of the crystallized solid phase, and n is the dimension of the crystal growth process. As expected from previous studies,[10,11,17,38] one can assume that the rate of (homogeneous) nucleation is proportional to the fraction, $f_a = 1 - f_c$ of the untransformed mother phase (gel),

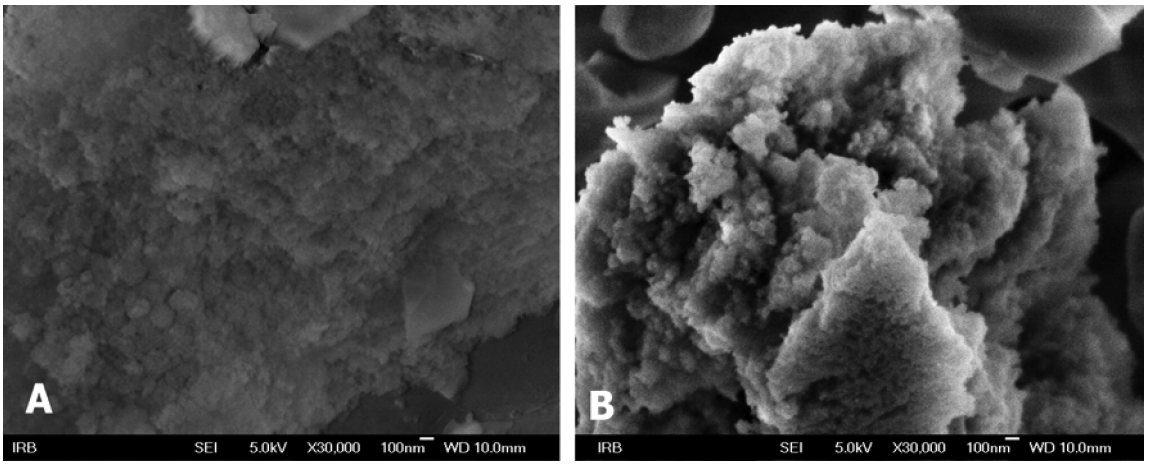

Figure 6. Scanning electron micrographs of leucite (A) and kalsilite (B) obtained by thermal treatment of precipitated amorphous precursors K-gel(A) and K-gel(B) at 1483 K, respectively.

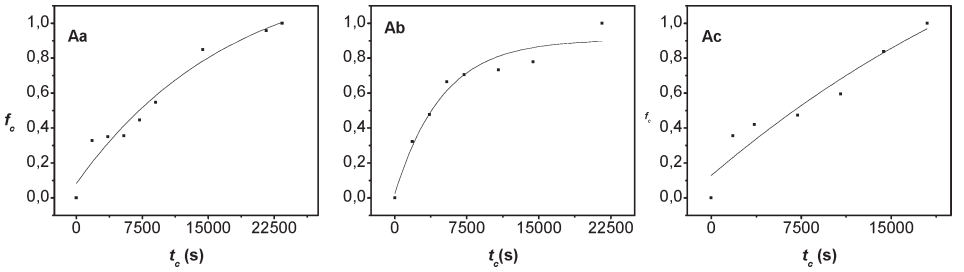

Figure 7. Changes in the measured mass fractions, f_c of leucite (symbols) and the mass fractions f_c calculated by eq 8, using the corresponding numerical values of K and m listed in Table 1. during isothermal heating of the precipitated amorphous aluminosilicate precursor K-gel(A) at 1423 (a), 1453 (b), and 1483 K (c).

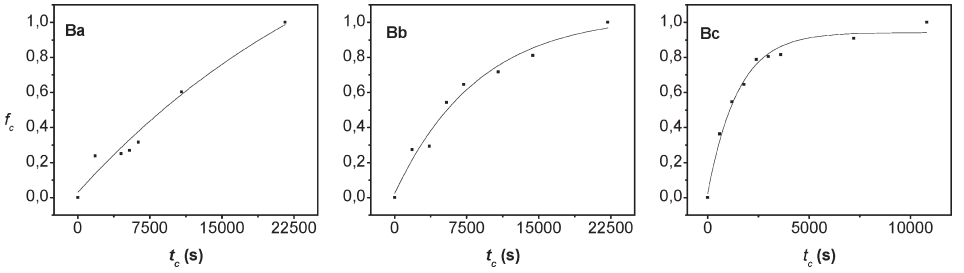

Figure 8. Changes in the measured mass fractions, f_c of kalsilite (symbols) and the mass fractions f_c calculated by eq 2, using the corresponding numerical values of K and m listed in Table 1 during isothermal heating of the precipitated amorphous aluminosilicate precursor K-gel(B) at 1423 (a), 1453 (b), and 1483 K (c).

that is,

$$dN/d\tau = K_n(1 - f_c) \quad (2)$$

and that the linear dimension $L(\tau,t)$ of the growing crystals is[40,42−45]

$$L(\tau, t) = [K_g(t - \tau)]^{1/p} \quad (3)$$

where $p = 1$ for a linear, size-independent crystal growth and $p = 2$ for a diffusion-controlled crystal growth. For the cases when only a fraction, $f_p^* < 1$, of the amorphous aluminosilicate can be transformed into the secondary phase, the rate of nucleation can be expressed as[10]

$$dN/d\tau = K_n(f_p^* - f_c) \quad (4)$$

Hence, a combination of eqs 1, 3, and 4 gives

$$df_c = G\sigma K_n(f_p^* - f_c)[K_g(t - \tau)]^n \, d\tau \quad (5)$$

where n = r/p and $r = 1$ for one-dimensional, $r = 2$ for two-dimensional, and $r = 3$ for three-dimensional crystal growth. Integration of the differential eq 4 gives[10,11,17]

$$f_c = f_p^* - f_p^* \exp\{-[G\sigma K_n(pK_g)^{r/p}/(1 + r/p)]\}t^{(1+r/p)}$$
$$= f_p^*[1 - \exp(-Kt^m)] \quad (6)$$

where $K = G\sigma K_n(pK_g)^{r/p}/(1 + r/p)$ and $m = 1 + r/p$. The short form of eq 6 with $f_p^* = 1$ is identical to the equation developed independently at about the same time by Kolomogorov,[45] Johnson and Mehl,[46] Avrami,[47] and Evans[48] (KJMAE equation). From eq 6, it is evident that $m = 2$, 3, or 4 for one-, two-, or three-dimensional linear size-independent growth and that $m = 3/2$, 2, or 5/2 for one-, two-, or three-dimensional diffusion-controlled growth. Hence, eq 6 can be used for kinetic analysis of the transformation of zeolites to amorphous aluminosilicates and their subsequent transformation

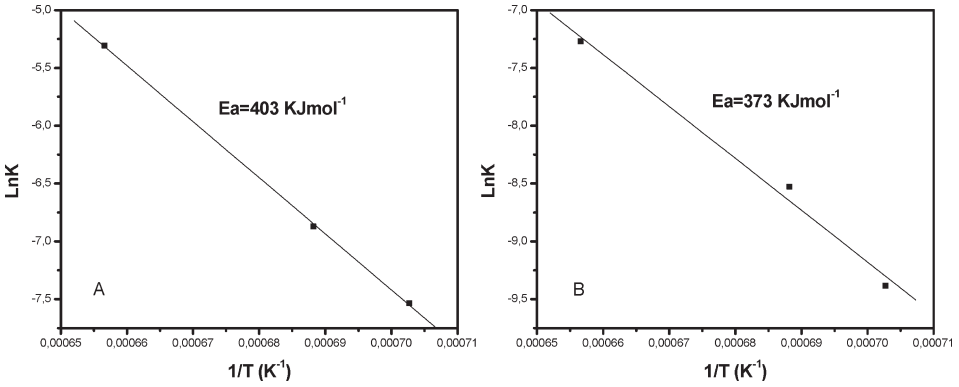

Figure 9. Arrhenius plot of isothermal crystallization of leucite (A) and kalsilite (B) from precipitated amorphous precursors K-gel(A) and K-gel(B), respectively.

Table 1. Numerical Values of the Constants *K* and *m* that Correspond to the Crystallization of Leucite and Kalsilite from the K-gel(A) and K-gel(B)

	T (K)	K	m
leucite	1423	5.341×10^{-4}	0.85−1
leucite	1453	1.037×10^{-3}	0.85−1
leucite	1483	4.955×10^{-3}	0.73−1
kalsilite	1423	8.400×10^{-5}	1.01−1
kalsilite	1453	1.978×10^{-4}	0.98−1
kalsilite	1483	6.962×10^{-4}	1.03−1

into secondary crystalline nonzeolitic phase(s)[11,17] as well as transformation of X-ray amorphous aluminosilicates into crystalline nonzeolitic crystalline phase(s).[10] Now, if eq 6 is relevant for the mathematical description of the crystallization of leucite from K-gel(A) and crystallization of kalsilite from K-gel(B), the values $\ln[-\ln(1 - f_c/f_p^*)]$ must be in a linear relationship with $\ln t$, that is,[10,11,17,44,49,50]

$$\ln[-\ln(1 - f_c/f_p^*)] = \ln K + m \ln t \quad (7)$$

where m is the slope and $\ln K$ is the intersection with y-axis of the straight line $\ln[-\ln(1 - f_c/f_p^*)]$ vs $\ln t$. All the values $\ln[-\ln(1 - f_c/f_p^*)]$ calculated from the measured fractions of f_c with $f_p^* = 0.8$ for K-gel(A) and $f_p^* = 0.85$ for K-gel(B) are in linear relationships with $\ln t$, thus indicating that eq 6 is relevant for the mathematical description of the crystallization of leucite from K-gel(A) and crystallization of kalsilite from K-gel(B). The corresponding values of K and m are listed in Table 1. Unexpected and surprisingly, the value of m is ~1 in all the analyzed cases, and thus,

$$f_c = f_p^*[1 - \exp(-K't)] \quad (8)$$

This can be valid in only two cases:

Model 1. $r = 0$, $n = r/p = 0$ ("zero-order" growth), and thus,

$$df_c = G\sigma K_n(f_p^* - f_c)[K_g(t - \tau)]^0 \, d\tau$$
$$= G\sigma K_n(f_p^* - f_c) \, d\tau \quad (9)$$

Integration of the differential eq 9 gives eq 8 with $K' = G\sigma K_n$. This implies formation of nuclei with the rate defined by eq 4, but without their subsequent growth. Such a less reliable process of transformation would result in the formation of agglomerates of nuclei of the crystalline phase. However, since the size of nuclei are assumed to be about 10 nm, and the size of the final product is 32 and 117 nm, respectively, this mechanism (formation of nuclei without their subsequent growth) is not relevant for the transformation process.

Model 2. $r > 0$, $n = r/p > 0$, $(t - \tau) = (t_x - \tau) = \Delta t =$ constant, and thus,

$$df_c = G\sigma K_n(f_p^* - f_c)[K_g(t_x - \tau)]^n \, d\tau$$
$$= G\sigma K_n(f_p^* - f_c)(K_g\Delta t)^n \, d\tau \quad (10)$$

Integration of the differential eq 10 gives eq 8 with $K' = G\sigma K_n(pK_g\Delta t)^{r/p}/(1 + r/p)$.

This mechanism implies that due the low mobility of the aluminosilicate building blocks the growth of the nuclei is limited by the spending of aluminosilicate materials in the vicinity of the nuclei. Since it can be assumed that all formed nanocrystals of the secondary crystalline phase have approximately the same size (for example, 32 nm in the case of leucite and 117 nm in the case of kalsilite), the time $\Delta t = t_x - \tau$ passed from the formation of nuclei at time τ until the spending of all the aluminosilicate material available for the growth of nuclei at the time t_x, is the same, that is, $\Delta t =$ constant. Hence, integration of the differential eq 10 gives eq 8 with $K' = G\sigma K_n(pK_g\Delta t)^{r/p}/(1 + r/p)$. Although both the models resulted in the same type of relationship between f_c and t, (see eq 8), due the above explained limitation, the growth according to Mechanism #2 is zero-order only apparently, and thus is denoted as pseudo-zero-order growth.

The asymptotic rate coefficients K are strongly temperature-dependent, as shown in Figure 9, which plots the usual Arrhenius plot of $\ln k$ versus $1/T$. The apparent activation energy (E_a) is calculated from the Arrhenius plot for both materials. The difference in activation energy (E_a for leucite and kalsilite crystallization was 403 and 373 kJ/mol, respectively) could be ascribed to the different primary and secondary units formed in the gel, as shown by different techniques, and also to the different way of the compounding as the crystal is being formed.

4. Conclusion

It was shown that aluminosilicate ceramics (kalsilite, leucite) can be obtained by a simple procedure, relatively cheaper than the conventional ones, namely, by thermal treatment of amorphous aluminosilicate precursors (gels). The potassium gels were prepared by two procedures: by the ion-exchange of sodium ions from sodium gel with potassium ions from solution (K-gel(A)) and by direct precipitation from K-aluminate and K-silicate solutions (K-gel(B)). Both the chemical composition and the microstructural properties of the gels depend on the method of preparation. Thermal

treatment of K-gel(A) (SiO_2/Al_2O_3 = 2.58) results in the formation of leucite (SiO_2/Al_2O_3 = 4) and thermal treatment of K-gel(B) (SiO_2/Al_2O_3 = 3.31) results in formation of kalsilite (SiO_2/Al_2O_3 = 2). This indicates that the type of formed ceramic is determined by microstructural properties of the precursor (gel) than by its chemical composition.

Kinetic analysis of the isothermal transformation process indicated that the rate of crystallization of leucite and kalsilite from the precipitated amorphous aluminosilicate can expressed as

$$f_c = f_p^* [1 - \exp(-K't)]$$

where f_c is the fraction of crystallized up to the time t. Although this kinetic equation implies the zero-order growth (formation of nuclei by homogeneous nucleation without their subsequent growth) the more detailed kinetic analysis showed that this kinetic equation can also be obtained in the case of limited growth, for example, when growth process is limited by the amount of aluminosilicate material in the vicinity of nuclei.

The apparent activation energy, E_a, of the crystallization of leucite and kalsilite from the precipitated amorphous aluminosilicate, calculated by the Arrhenius equation (i.e., from the slope of ln K vs $1/T$ straight line), was 403.32 kJ/mol and 373.10 kJ/mol, respectively.

The higher apparent activation energy (E_a = 403 kJ/mol) of the crystallization of leucite relative to the apparent activation energy (E_a = 373 kJ/mol) of the crystallization of kalsilite from the precipitated amorphous aluminosilicate precursors is caused by more heterogeneous distribution of Si and Al in the precipitated amorphous aluminosilicate precursor K-gel-(A) than in the precipitated amorphous aluminosilicate precursor K-gel(B).

Acknowledgment. The authors thank the Ministry of Science of the Republic of Croatia and Slovenian Ministry of Education, Science and Sport for their financial support.

Supporting Information Available: Supplementary Figure 2A−C. This material is available free of charge via the Internet at http://pubs.acs.org.

References

(1) Mimura, H.; Kanno, T. *Sci. Rep. RITU 29A* **1980**, 102–111.
(2) Dondur, V.; Dimitrijević, R. *J. Solid State Chem.* **1982**, *62*, 46–51.
(3) Subramanian, M. A.; Corbin, D. R.; Chowdhry, U. *Adv. Ceram.* **1989**, *26*, 239–247.
(4) Subramanian, M. A.; Corbin, D. R.; Chowdhry, U. *Bull. Mater. Sci.* **1993**, *16*, 665–678.
(5) Bedard, R. L.; Broach, R. W.; Flanigen, E. M. *Proc. Symp. Better Ceramics Through Chemistry V*; In Hampden-Smith, M. J., Klemperer, W. G., Brinker, C. J., Eds.; Material Research Society: Pittsburgh, PA, 1992; pp 581−587.
(6) Hoghooghi, B.; McKittrick, J.; Butler, C.; Desch, P. *J. Non-Cryst. Solids* **1994**, *170*, 309–317.
(7) Kosanović, C.; Subotić, B.; Šmit, I.; Čižmek, A.; Stubičar, M.; Tonejc, A. *J. Mater. Sci.* **1997**, *32*, 73–78.
(8) Del'Agli, G.; Ferone, C.; Mascolo, M. C.; Pansini, M. *Solid State Ionics* **2000**, *127*, 309–317.
(9) Kosanović, C.; Subotić, B.; Ristić, A. *Croat. Chem. Acta* **2002**, *75*, 783–792.
(10) Kosanović, C.; Subotić, B.; Kranjc, E. *Microporous Mesoporous Mater.* **2004**, *71*, 27–32.
(11) Kosanović, C.; Subotić, B.; Ristić, A. *Mater. Chem. Phys.* **2004**, *86*, 390–398.
(12) Kosanović, C.; Subotić, B. *Microporous Mater.* **1997**, *12*, 261–266.
(13) Kosanović, C.; Subotić, B.; Kaučič, V.; Škreblin, M. *Phys. Chem. Chem. Phys. 2* **2000**, 3447–3451.
(14) Kosanović, C.; Subotić, B. *Microporous Mesoporous Mater.* **2003**, *66*, 311–319.
(15) Kosanović, C.; Subotić, B.; Šmit, I. *Thermochim. Acta* **1998**, *317*, 25–37.
(16) Kosanović, C.; Bosnar, S.; Subotić, B.; Novak Tušar, N.; Ristić, A.; Gabrovšek, R.; Kaučič, V. *Microporous Mesoporous Mater.* **2008**, *112* (1−3), 542–552.
(17) Kosanović, C.; Subotić, B.; Ristić, A.; Sekovanić, L. *Croat. Chem. Acta* **2004**, *77*(4), 553−560.
(18) Correns, C. W. *Introduction to Mineralogy*; Springer: New York, 1969.
(19) Hermans, P. H.; Weidinger, A. *Makromol. Chem.* **1961**, *44/46*, 24–48.
(20) Zevin, L. S.; Zavyalova, L. L. *Kolichestvenniy Rentgenographicheskiy Prazovij Analiz*; Nedra: Moscow, 1974; p 37.
(21) Zhdanov, S. P. *Adv. Chem. Ser.* **1971**, *101*, 20–23.
(22) Engelhardt, G.; Fahlke, B.; Mägi, M.; Lippmaa, E. *Zeolites* **1983**, *3*, 292–294.
(23) Lippmaa, E.; Mägi, M.; Samson, A.; Engelhardt, G.; Grimmer, A.-R. *J. Am. Chem. Soc.* **1981**, *102*, 4889–4895.
(24) Katović, A.; Subotić, B.; Šmit, I.; Despotović, L. J. A.; Ćurić, M. *ACS Symp. Ser. 398*; American Chemical Society: Washington, DC, 1989; pp 124−129.
(25) Gonthier, S.; Gora, L.; Guüray, I.; Thompson, R. W. *Zeolites* **1993**, *13*, 414–418.
(26) Dutta, P. K.; Puri, M.; Bowers, C. Zeolite Synthesis, In Occelli, M. L.; Robson, H. E., Eds.; *ACS Symp. Ser. No. 398*; American Chemical Society: Washington, DC, 1989, pp 98−104.
(27) Walton, R. I.; Smith, R. I.; O'Hare, D. *Microporous Mesoporous Mater.* **2001**, *48*, 79–88.
(28) *Recent Progress Report and Discussions: 5th International Zeolite Conference*, Naples, Italy, 1980; Bursill, L. A.; Thomas, J. M.; Sersale, R.; Collela, C.; Aiello, R., Eds.; Giannini: Naples, 1981; pp 25−30.
(29) Nikolakis, V.; Vlachos, D. G.; Tsapatsis, M. *Microporous Mesoporous Mater.* **1998**, *21*, 337–346.
(30) Kosanović, C.; Bosnar, S.; Subotić, B.; Svetličić, V.; Mišić, T.; Dražić, G.; Havenscak, K. *Microporous Mesoporous Mater.* **2008**, *110*, 177–185.
(31) Kosanović, C.; Havancsak, K.; Subotić, B.; Svetli čić, V.; Mišić, T.; Cziraki, A.; Huhn, G. *Microporous Mesoporous Mater.* **2009**, *123*, 150–159.
(32) Erdem, A.; Sand, L. B. *Proceedings of the 5th International Conference on Zeolites*; Rees, L. V. C., Ed.; Heyden: London, 1980; p 64.
(33) Gabelica, Z.; Blom, N.; Derouane, E. G. *Appl. Catal.* **1983**, *5*, 227–248.
(34) Nastro, A.; Aiello, R.; Colella, C. *Ann. Chim.* **1984**, *74*, 579–587.
(35) Aiello, R.; Crea, F.; Nastro, A.; Pellegrino, C. *Zeolites* **1987**, *7*, 594.
(36) Aiello, R.; Crea, F.; Nastro, A.; Subotić, B.; Testa, F. *Zeolites* **1991**, *11*, 767–775.
(37) Subotić, B., Tonejc, A. M., Bagović, D., Čižmek, A., Antonić, T. In *Zeolites and Related Microporous Materials: State of Art 1994*; Weitkamp, J.; Karge, H. G.; Pfeifer, H.; Hoeldrich, W., Eds.; Studies in Surface Science and Catalysis No. 94A, Elsevier: Amsterdam, 1994; pp 259−266.
(38) Von Goler, F.; Sachs, G. *Z. Phys.* **1932**, *77*, 281–287.
(39) Mendelkern, L. *Crystallization of Polymers*; McGraw-Hill: New York, 1964; pp 215−228.
(40) Gualtieri, A. F. *Phys. Chem. Miner.* **2001**, *28*, 719–728.
(41) Nielsen, A. E. *Croat. Chem. Acta* **1980**, *53*, 255–279.
(42) Brečević, Lj., Kralj, D. *Interfacial Dynamics*, in Kallay, N., Ed.; Marcel Dekker Inc.: New York, 1999; pp 435−474.
(43) Woldt, E. *Metall. Mater. Trans. A* **2001**, *32*, 2465–2473.
(44) Rutenberg, G.; Woldt, E.; Petford-Long, A. K. *Thermochim. Acta* **2001**, *378*, 97–105.
(45) Kolomogorov, A. N. *Izv. Akad. Nauk. SSSR, Ser. Mater.* **1937**, *3*, 355–360.
(46) Johnoson, W. A.; Mehl, R. F. *Trans. AIME 135* **1939**, 416–458.
(47) Avrami, M. *J. Phys. Chem.* **1939**, *7*, 1103–1113.
(48) Evans, U. R. *Trans. Faraday Soc.* **1945**, *41*, 365–372.
(49) Lopez-Alemany, P. L.; Vasquez, J.; Villares, P.; Jimenez-Garay, R. *Thermochim. Acta* **2001**, *374*, 73–78.
(50) Boutarfaia, A.; Legouera, M.; Poulain, M. *J. Non-Cryst. Solids* **2001**, *291*, 176–181.